PERGAMON

International Journal of Multiphase Flow 25 (1999) 1575–1599

International Journal of Multiphase Flow

www.elsevier.com/locate/ijmulflow

Stochastic simulations of particle-laden isotropic turbulent flow

Farzad Mashayek *

Department of Mechanical Engineering, University of Hawaii at Manao, 2540 Dole Street, Honolulu, HI 96822, USA

Received 9 July 1997; received in revised form 9 November 1998

Abstract

Numerical simulations are performed of dispersion and polydispersity of particles in isotropic incompressible turbulence. The mass loading of the particles is assumed to be small; thus the effects of particles on turbulence is neglected (one-way coupling). A stochastic model is employed to simulate the carrier phase. The results of the simulations are compared with direct numerical simulation (DNS) data and theoretical results. The stochastic model predicts most of the trends as portrayed by DNS and theory. However, the continuity effect associated with the crossing trajectories effect is not captured. Also, the peaking in the variation of the particle asymptotic diffusivity coefficient with the particle time constant is not observed. For evaporating particles, the stochastic model predicts thinner probability density functions (pdfs) for the particle diameter as compared with DNS generated pdfs. The model is implemented to investigate the effects of gravity on evaporation. It is shown that the depletion rate increases with increase of the drift velocity at short and intermediate times, but an opposite trend is observed at long times. The standard deviation and skewness of the particle diameter indicate peak values in their variations with the drift velocity. Dispersion of evaporating particles decreases with respect to that of non-evaporating particles at small drift velocities; an opposite trend is observed at large drift velocities. The effects of the initial evaporation rate and the particle Schmidt number on the evaporation in the gravity environment are also studied.

Keywords: Stochastic simulation; Isotropic turbulence; Gravity; Particle dispersion; Polydispersity

1. Introduction

In stochastic modelling of particle-laden flows, an ensemble of physical particles is considered in conjunction with some assumptions pertaining to the turbulent flow field. The

* Tel.: +1-808-956-9693; fax: +1-808-956-2373; e-mail: mashaye@wiliki.eng.hawaii.edu.

0301-9322/99/$ - see front matter
PII: S0301-9322(98)00076-7

particles can be considered as "Monte Carlo" computational elements which are expected to portray the physics of turbulent dispersion in a statistical manner. In this way, the flow field is not exactly calculated; rather its stochastic "realizations" are attempted. One of the early stochastic models of turbulent dispersion is due to Gosman and Ioannides (1981). In this model, the turbulence is assumed to be isotropic and to have a Gaussian pdf with the variance of $2k/3$, where k is the turbulence kinetic energy. The fluctuating fluid velocity along the particle trajectory is randomly sampled from the Gaussian pdf and the particle is allowed to interact with an eddy over a time interval which is the minimum of two time scales: the turbulent eddy life-time, and the residence time of the particle within the eddy. This model was also implemented by Shuen et al. (1983, 1985) and Solomon et al. (1984) to predict particle-laden jets, and by Graham and James (1996), who discuss the effects of the model parameters and the initial conditions.

The model of Gosman and Ioannides (1981) does not account for the temporal correlations and directional anisotropies associated with turbulent flows. This could result in some inaccuracies in capturing some of the well-established features of dispersion, such as the crossing trajectories effect. An improved model is proposed by Ormancey and Martinon (1984) which accommodates for both the temporal and the spatial structures of turbulence. In this model, the trajectories of massless fluid particles are constructed by integrating their Lagrangian equations. Associated with each fluid particle is a "fluid domain" centered at the fluid particle location. A heavy particle can follow a fluid domain or can move from one fluid domain to another, accounting for the effect of crossing trajectories. Within the fluid domain, the fluid velocity fluctuation at the particle location is taken from a random sample with specified one- and two-point correlations. A particle remains within one fluid domain as long as its distance from the fluid particle is smaller than some pre-defined length, or until the turbulent structure around the fluid particle vanishes by exceeding the random life-time of the fluid domain. The sizes and life-times of fluid domains are determined by length and time scales of turbulence. A similar model is proposed by Berlemont et al. (1990, 1991). However, this latter model allows the choice of different shapes for the correlation function, in contrast to the model of Ormancey and Martinon (1984) in which the shape of the Lagrangian correlation function is a consequence of the stochastic process used. Parthasarathy and Faeth (1990) use a stochastic model to predict dispersion of particles in self-generated homogeneous turbulence. This model is based on the idea of time series analysis of Box and Jenkins (1976) to satisfy the mean and fluctuating velocities and Lagrangian time correlations of the velocity fluctuations. Parthasarathy and Faeth (1990) report good agreement between the model predictions and experimental data.

In this work, we consider the stochastic model proposed by Lu (1995). This model, similarly to that of Ormancey and Martinon (1984), accounts for the temporal and spatial correlations. However, instead of constructing the trajectories of fluid particles through the correlations at several time steps, only the correlation between two successive time steps is considered. As a result, the implementation of the model is somewhat easier and requires less bookkeeping effort. Also, by using the Eulerian (as opposed to the Lagrangian) autocorrelation, the model is capable of producing the same trend for the variation of the particle diffusivity coefficient as those predicted by theory (e.g. Pismen and Nir, 1978). Lu (1995) reports good agreements between the model predictions and experimental data of Snyder and Lumley (1971). Here, we

assess the performance of the model via comparisons with DNS data of Mashayek et al. (1997) and theoretical results of Mei et al. (1991) in isotropic incompressible particle-laden turbulent flows. The model is also implemented to investigate the effects of gravity on polydispersity of evaporating particles. The stochastic model is briefly described in Section 2, following the problem formulation. The model predictions are compared with the results of DNS and theory in Sections 3 and 4, respectively. In Section 5 the effects of gravity on evaporation is analyzed followed by the summary and concluding remarks in Section 6.

2. Formulation

We consider the motion of spherical particles in an incompressible and isotropic turbulent flow. It is assumed that the dispersed phase is very dilute, thus the effect of particles on the carrier fluid is negligible. The momentum equation for each particle is considered in the Lagrangian frame of reference. In general, this equation contains the Stokes drag, the Basset force, the force due to fluid pressure gradient, the inertia force of added mass, and the gravity (Maxey and Riley, 1983). However, if the ratio of the density of the particle to the density of the carrier fluid is large, the inertia, the Stokes drag, and the gravity forces are dominant and the other forces can be assumed negligible. With this assumption the governing equations for a single particle are expressed as

$$\frac{\mathrm{d}\mathbf{v}}{\mathrm{d}t} = \frac{18\mu}{\rho_\mathrm{p} d_\mathrm{p}^2}(\mathbf{u} - \mathbf{v}) + g\mathbf{e} \tag{1}$$

$$\frac{\mathrm{d}\mathbf{X}}{\mathrm{d}t} = \mathbf{v} \tag{2}$$

where **u** and **v** (boldface indicates vector) denote the fluid velocity at the particle location and the particle velocity, respectively; t is time, **X** is the center position of the particle, **e** is the unit vector in the gravity direction, g is the gravity constant; ρ_p and d_p denote the particle density and diameter, respectively; and μ is the fluid viscosity. All the variables are normalized by reference scales of length, L_0, velocity, U_0, and density, ρ_0. Later in this paper we also consider a modified Stokes drag relation for large particle Reynolds numbers.

In the simulations of non-evaporating (solid) particles, the particle diameter remains constant. For evaporating particles, the rate of diameter reduction is modeled by the d^2-law (Turns, 1996)

$$d_\mathrm{p}^2 = d_{\mathrm{p}0}^2 - kt \tag{3}$$

where $d_{\mathrm{p}0}$ is the initial diameter of the particle and the depletion rate is given by: $k = 8\Gamma \ln(1 + B_\mathrm{M})C_{Re}$, where Γ is the mass diffusivity coefficient and B_M is the transfer number (Spalding, 1953). The parameter $C_{Re} = 1 + 0.3Re_\mathrm{p}^{0.5}Sc_\mathrm{p}^{0.33}$ is a correction factor to account for the convective effects (Ranz and Marshall, 1952) with Re_p and Sc_p representing the particle Reynolds and Schmidt numbers, respectively. The flow is assumed isothermal and evaporation is due to a constant temperature difference between the drop and the fluid. This model is in

accord with that of several laboratory experiments (e.g. Shearer et al., 1979). In a dilute flow, the ratio of the mass of the particle to the mass of the carrier fluid is very small and it is assumed that the particles are in contact with the carrier fluid during evaporation. Therefore, the transfer number B_M is the same for all the particles, and the variation of k is only due to the parameter C_{Re}. A relation for the "particle time constant" (τ_p) is obtained from Eq. (3)

$$\tau_p(t) = \frac{\rho_p d_p^2}{18\mu} = \tau_{p0} - \tau_e t \tag{4}$$

where $\tau_{p0} = (\rho_p d_{p0}^2)/18\mu$ denotes the initial particle time constant, and

$$\tau_e = \tau_{e0} C_{Re}, \quad \tau_{e0} = \frac{4\rho_p \Gamma}{9\mu} \ln(1 + B_M) \tag{5}$$

For convenience, the largest evaporation rate is chosen such that the particle velocity autocorrelation approaches zero by the time $\tau_p = 0.1\tau_{p0}$ (about 3.1 eddy turnover times). Therefore: $\tau_{e0} = 0.9\tau_{ec}/3.1 = 0.29\tau_{ec}$ where τ_{ec} is introduced to relate the evaporation rate to the initial particle time constant. It should be mentioned that the parameter τ_{ec} does not bear a specific physical significance. It is only produced from a computational point of view to insure that very small values of the particle time constant are not encountered during the simulations. By introducing a drift velocity, $\upsilon_{dr} = \tau_{p0} g$, Eq. (1) is expressed as

$$\frac{d\mathbf{v}}{dt} = \frac{1}{\tau_p}(\mathbf{u} - \mathbf{v}) + \frac{1}{\tau_{p0}} \upsilon_{dr} \mathbf{e} \tag{6}$$

The particle Reynolds number is defined as: $Re_p = (\rho_f d_p |\mathbf{u} - \mathbf{v}|)/\mu$ with ρ_f denoting the carrier fluid density. Following Wang and Maxey (1993) the Reynolds number is related to the flow Kolmogorov time scale (τ_k) and velocity scale (υ_k) with $\nu = \tau_k \upsilon_k^2$, where $\nu = \mu/\rho_f$ is the fluid kinematic viscosity

$$Re_p = \left(\frac{18\tau_p}{\nu\rho_p/\rho_f}\right)^{1/2} |\mathbf{u} - \mathbf{v}| = 4.243 \left(\frac{\rho_f}{\rho_p}\right)^{1/2} \left(\frac{\tau_p}{\tau_k}\right)^{1/2} \frac{|\mathbf{u} - \mathbf{v}|}{\upsilon_k} \tag{7}$$

For large particle Reynolds numbers a "modified" Stokes drag must be used. The modification is in the form of an empirical correction factor which is multiplied by the Stokes drag relation. The empirical correction factor is described as a function of the particle Reynolds number ($f(Re_p)$) and can be easily implemented in Eq. (6) by replacing τ_p with a modified particle time constant, $\tau_p^* = \tau_p/(f(Re_p))$. A variety of relations for $f(Re_p)$ is available (Clift et al., 1978); here we use

$$f(Re_p) = 1 + 0.15\ Re_p^{0.687} \tag{8}$$

The particles can be tracked in the Lagrangian frame by integrating Eqs. (6) and (2) provided that the fluid velocity at the particle location is known. Here, we use the stochastic model proposed by Lu (1995) to simulate the fluid velocity. The rudiments of the model are taken from the methodology of time series analysis (Box and Jenkins, 1976). Let the coordinate system move with the mean velocity; thus, only the fluctuating velocities are considered. The

particle position, $X_i(0)$, $i = 1, 2, 3$ and velocity, $v_i(X_i(0), 0)$, are given at the starting time $t = 0$. The initial fluid velocity, $u_i(X_i(0), 0)$, at the particle location is extracted from a random Gaussian seed with the standard deviation u' (assumed to be known a priori). Then, the particles are moved to their new positions, $X_i(\Delta t)$ (Δt is the time increment), using a second-order Runge–Kutta method. In order to advance the calculations for the next time step, the fluid velocity, $u_i(X_i(\Delta t), \Delta t)$, at the new particle location must be found. By the time particles arrive at their new locations, the fluid velocity at the old particle location changes to $u_i(X_i(0), \Delta t)$. To relate the old and the new fluid velocities at $X_i(0)$, the Eulerian velocity autocorrelation

$$F_{\alpha\alpha}(\Delta t) = \frac{\langle w_\alpha(X_\alpha(0), 0) w_\alpha(X_\alpha(0), \Delta t)\rangle}{\langle w_\alpha(X_\alpha(0), 0) w_\alpha(X_\alpha(0), 0)\rangle}, \quad \alpha = 1, 2, 3 \tag{9}$$

(with no summation over repeated Greek indices) is used, where $w_i = u_i/u'$ is the normalized velocity and $\langle\ \rangle$ indicates the ensemble average. It is also necessary to account for the spatial separation between the fluid particle and the heavy particle locations through the Eulerian spatial correlation

$$G_{\alpha\alpha}(\Delta s) = \frac{\langle w_\alpha(X_\alpha(0), \Delta t) w_\alpha(X_\alpha(\Delta t), \Delta t)\rangle}{\langle w_\alpha(X_\alpha(0), \Delta t) w_\alpha(X_\alpha(0), \Delta t)\rangle}, \quad \alpha = 1, 2, 3 \tag{10}$$

where $\Delta s = |\mathbf{X}(\Delta t) - \mathbf{X}(0)|$ is the distance between the old and the new particle locations. To use Eq. (10), it is necessary to re-orient the coordinate system such that one of the axes coincides with $\mathbf{X}(\Delta t) - \mathbf{X}(0)$.

By defining autoregressive processes (Box and Jenkins, 1976) (in time) for $w_i(X_i(0), 0)$ and $w_i(X_i(0), \Delta t)$, and (in space) for $w_i(X_i(0), \Delta t)$ and $w_i(X_i(\Delta t), \Delta t)$, with some algebraic manipulations, Lu (1995) obtains

$$w_\alpha(X_\alpha(\Delta t), \Delta t) = a_\alpha b_\alpha w_\alpha(X_\alpha(0), 0) + \gamma_\alpha, \quad \alpha = 1, 2, 3 \tag{11}$$

where $a_\alpha = F_{\alpha\alpha}(\Delta t)$, $b_\alpha = G_{\alpha\alpha}(\Delta t)$ and γ_α is a Wiener process which is determined by its variance, $\sigma_{\gamma\alpha} = \sqrt{1 - a_\alpha^2 b_\alpha^2}$. Once the fluid velocity at the new particle location is determined using Eq. (11), the steps described above are repeated and the particle trajectory is constructed.

The following relations are used for the Eulerian temporal and spatial correlations (Lu, 1995): $F_{\alpha\alpha}(\Delta t) = \exp(-\Delta t/\tau_E)$, $G_{11}(\Delta s) = \exp(-\Delta s/\Lambda_1)$, $G_{22}(\Delta s) = G_{33}(\Delta s) = \exp(-\Delta s/\Lambda_2)$, where τ_E is the Eulerian integral time scale and Λ_1 and Λ_2 are the Eulerian integral length scale in the longitudinal and transverse directions, respectively. In isotropic incompressible flows, these are estimated by:

$$\tau_L = C\frac{(u')^2}{\epsilon}, \quad \tau_E = \frac{\tau_L}{C_2}, \quad \Lambda_1 = 2\Lambda_2 = C_3\tau_L u',$$

where τ_L is the Lagrangian integral time scale, ϵ is the dissipation rate, and $C_1 = 0.212$, $C_2 = 0.73$, $C_3 = 2.778$. The values used for C_1 and C_3 are the same as those suggested by Lu (1995). The value of C_2 is larger than that used by Lu (1995), and is the upper limit found in the literature (Hinze, 1975). The results produced by $C_2 = 0.73$ are within approximately 10% of those obtained using the value proposed by Lu (1995) and indicate better agreements with the results of theory and DNS.

With this formulation, the values of the fluid turbulence intensity and dissipation rate of the turbulence kinetic energy are model inputs. The values $u' = 0.0185$ and $\epsilon = 3.987\times10^{-6}$ are taken from DNS of Mashayek et al. (1997). For these values, the length scale is conveniently chosen such that the normalized size of the simulation box for DNS is 2π, the velocity scale is found from the box Reynolds number, $Re_0 = (\rho_0 U_0 L_0)/\mu_0$, and the fluid density is used as the scale for density. In the presentation of results, the particle variables are normalized by fluid variables. The choice of the time step depends on various parameters such as the Eulerian integral time scale and the particle time constant. Lu (1995) elaborates on the sensitivity of the model to the time step and (via extensive simulations) finds the range of Δt for which the results become independent of the time step. For the cases presented in this paper, the appropriate time step is found by performing numerical experiments with various Δt. Similar to findings of Lu (1995), our trial simulations indicated that the results vary negligibly for a wide range of variation of the time step. In all cases, 25^3 particles are tracked.

3. Model assessment via comparison with DNS

Recently, Mashayek et al. (1997) have performed extensive DNS to investigate dispersion (and polydispersity) of solid (and evaporating) particles in stationary isotropic incompressible turbulence. This configuration provides an ideal setting for the assessment of the stochastic model. In this section, the DNS results of Mashayek et al. (1997) are used for this assessment. In doing so, the primary consideration is to re-scale the DNS generated time and velocity scales to those of stochastic simulations via (Elghobashi and Truesdell, 1992):

$$\frac{\tau_p}{\tau_E}\Big)_{DNS} = \frac{\tau_p}{\tau_E}\Big)_{STH} \quad \text{and} \quad \frac{\tau_g}{\tau_E}\Big)_{DNS} = \frac{\tau_g}{\tau_E}\Big)_{STH}$$

where $\tau_g = d_p/\upsilon_{dr}$ is the drift timescale and STH refers to stochastic simulation. The reasoning for considering the fluid eddy turnover time for scaling is discussed by Elghobashi and Truesdell (1992). This adjustment is necessary as the stochastic model, by nature, is designed for Reynolds numbers higher than those attainable by DNS.

3.1. Dispersion of solid particles

First, we consider dispersion of solid (non-evaporating) particles. In Fig. 1 the particle velocity autocorrelation coefficients,

$$R^p_{\alpha\alpha}(t) = \frac{\langle \upsilon_\alpha(0)\upsilon_\alpha(t)\rangle}{\langle \upsilon^2_\alpha(0)\rangle}, \quad \alpha = 1, 2, 3 \tag{12}$$

as generated by DNS are compared with those by stochastic simulations for various particle time constants. For direct comparisons with DNS results, the particle time constant and the drift velocity are expressed in terms of the Kolmogorov time and velocity scales, respectively. In the absence of gravity, Fig. 1a shows that the agreement between the particle velocity autocorrelations is very good for large particles. However, as the particle time constant is

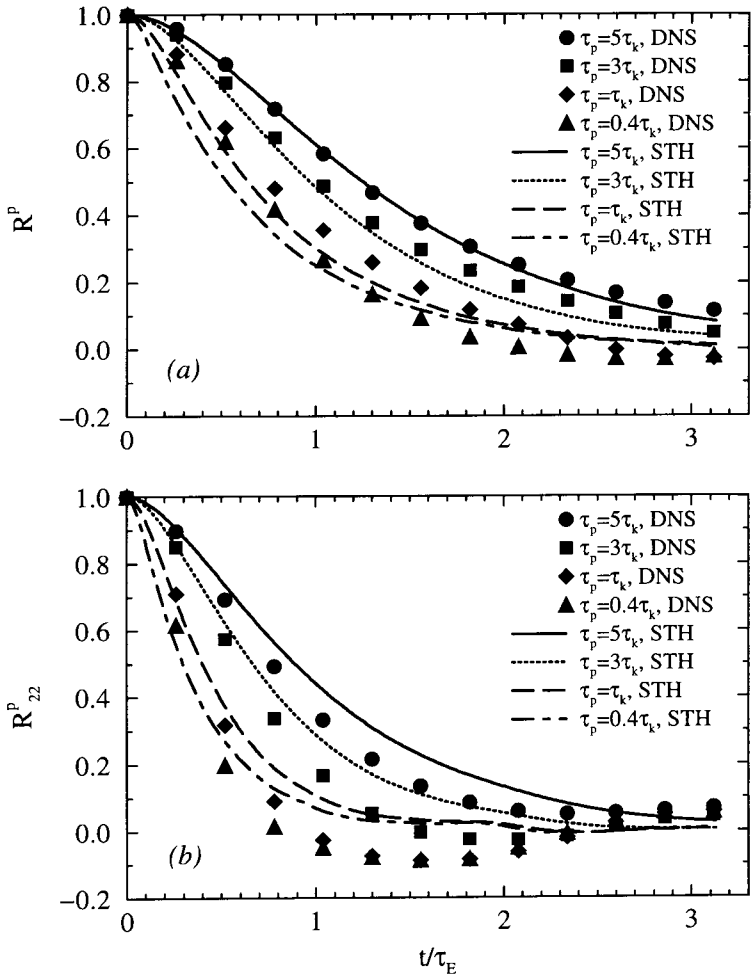

Fig. 1. Temporal variations of the particle velocity autocorrelation coefficient from the stochastic and direct numerical simulations. (a) In the absence of gravity, $R^p = \frac{1}{3}(R^p_{11} + R^p_{22} + R^p_{33})$. (b) For $v_{dr} = 5v_k$, in the direction normal to the gravity direction.

decreased, the results of stochastic simulations deviate from DNS results. At very small particle time constant ($\tau_p = 0.4\tau_k$) the stochastic model underestimates DNS results at short times and overestimates them at longer times. The agreement is weaker in the presence of gravity (Fig. 1b for $v_{dr} = 5v_k$) and significant deviations are observed for all particle time constants. It appears that the stochastic model does not predict the negative loops in the particle velocity autocorrelation curve. These loops are due to the continuity effect (Csanady, 1963) associated with the crossing trajectories effect. Therefore, while the effects of crossing trajectories are portrayed (as witnessed by the decrease of the particle velocity autocorrelation coefficient with the increase of the drift velocity), the continuity effects are not captured by the model.

The particle turbulence intensities calculated from the stochastic model are compared against DNS data for a variety of particle time constants and drift velocities in Fig. 2. These quantities

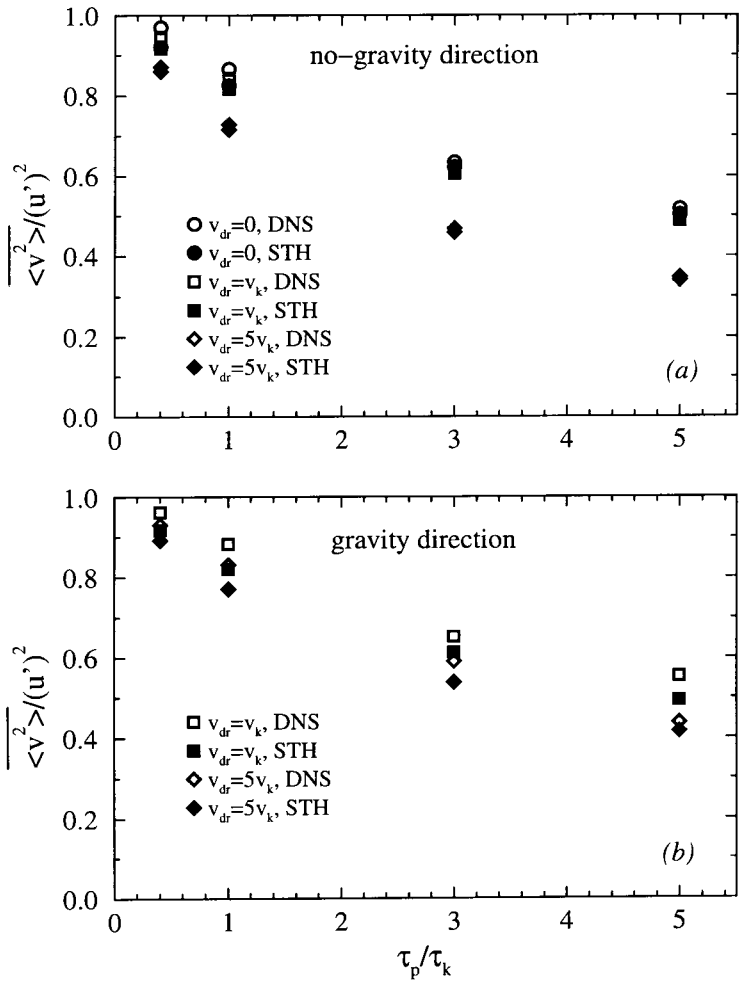

Fig. 2. Particle turbulence intensity from stochastic simulations and DNS, in the direction (a) normal and (b) parallel to the gravity direction.

are time averaged (indicated by an overbar) over more than three eddy turnover times in both simulations. As expected, with the increase of the particle's inertia, its tendency to follow turbulent fluctuations is diminished and the particle turbulence intensity is decreased. Also, the increase of the drift velocity results in the decrease of the particle turbulence intensity due to the crossing trajectories effect. The general trends shown in Fig. 2 have been observed by others (see e.g. Snyder and Lumley, 1971; Wells and Stock, 1983; Mei et al., 1991). Fig. 2 indicates that the agreement between the model predictions and DNS results is good in both of the directions parallel and normal to the gravity direction. No apparent preference towards either small or large particles is observed. This is interesting as the scaling between the two simulations is based on the large scale eddy turnover time and the smaller particle time constants are of the order of the Kolmogorov time scale. Also, the good agreement observed in

the presence of gravity indicates that the incapability of the stochastic model to account for the continuity effects does not affect the calculation of the particle turbulence intensity.

Fig. 3 presents the asymptotic particle turbulence diffusivity coefficient, $\epsilon^{\mathrm{p}} = D^{\mathrm{p}}(t \to \infty)$, in both the presence and the absence of gravity. In accord with DNS, the particle diffusivity coefficient, $D^{\mathrm{p}}(t) = [D^{\mathrm{p}}_{11}(t) + D^{\mathrm{p}}_{22}(t) + D^{\mathrm{p}}_{33}(t)]/3$, is determined by (Hinze, 1975)

$$D^{\mathrm{p}}_{\alpha\alpha}(t) = \langle \upsilon^2_\alpha(0)\rangle \int_0^t R^{\mathrm{p}}_{\alpha\alpha}(\tau)\mathrm{d}\tau = \int_0^t \langle \upsilon_\alpha(0)\upsilon_\alpha(\tau)\rangle \mathrm{d}\tau \quad \alpha = 1, 2, 3 \tag{13}$$

The results (not shown) for the diffusivity coefficients of the fluid particle surrounding the heavy particle exhibit similar trends to those observed in Fig. 3. The asymptotic values are

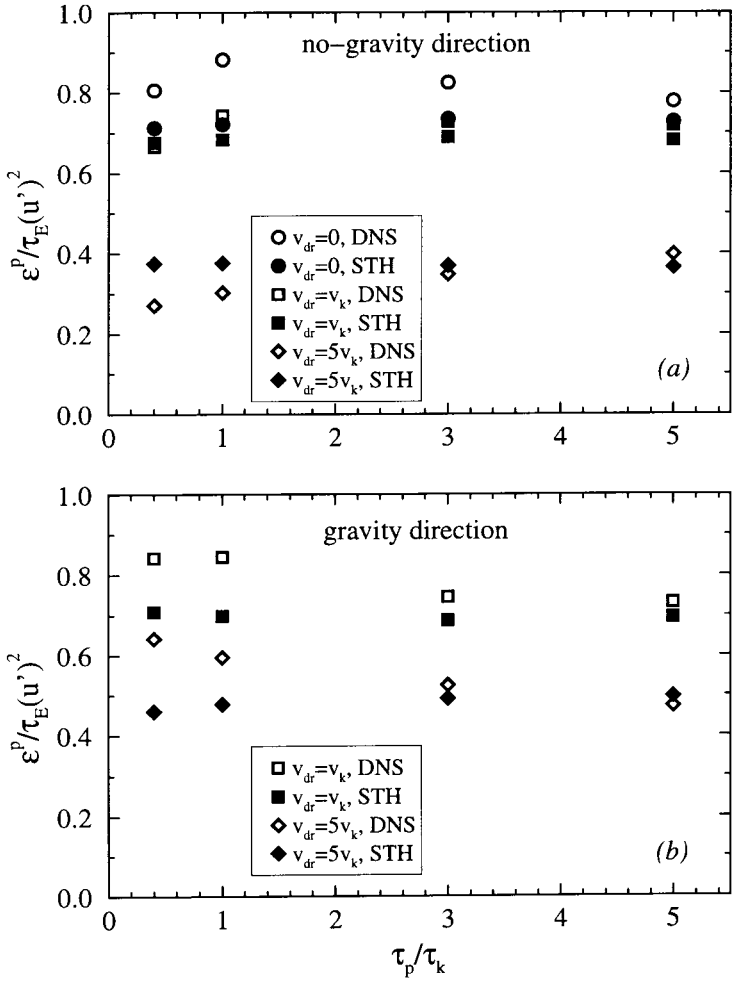

Fig. 3. Particle asymptotic diffusivity coefficient from stochastic simulations and DNS in the direction (a) normal and (b) parallel to the gravity direction.

calculated based on a "finite" time (about 3.5 eddy turnover times) in both DNS and stochastic simulations. The results in Fig. 3 show that, contrary to the particle turbulence intensity, the asymptotic particle diffusivity coefficients are predicted with some deviations from those calculated by DNS. The extent of deviation is increased as the particle time constant is decreased. This is not an artifact of using a finite time to calculate the asymptotic values, as with the decrease of the particle time constant the velocity autocorrelation approaches zero in a shorter time. Therefore, the asymptotic values are reached in a shorter time and smaller deviations are expected at smaller particle time constants. Fig. 3 shows that the general trends in the variations of the particle diffusivity coefficient with the drift velocity are captured by the stochastic model. However, the model does not predict the peak value in the variation of the particle diffusivity coefficient with the particle time constant. The peak value in DNS occurs for particle time constants of the order of the Kolmogorov time scale and is due to the increase of the effects of the preferential collection of particles in high strain regions of the flow at these small particle time constants. This suggests that this model can be more safely used for particle time constants of the order of the larger time scales of the flow.

3.2. Polydispersity of evaporating particles

When the particles evaporate, their interaction with the carrier fluid results in a distribution of particle sizes. This is the case even if initially all the particles are of the same size. Since the evaporation rate is strongly controlled by the instantaneous particle Reynolds number, it is instructive to first consider the temporal variations of the particle Reynolds number for non-evaporating particles at different particle time constants. Fig. 4 provides a comparison between the particle Reynolds numbers calculated using the stochastic model with those from DNS. By examining this figure it is realized that: (i) the initial time required by the particles to reach the

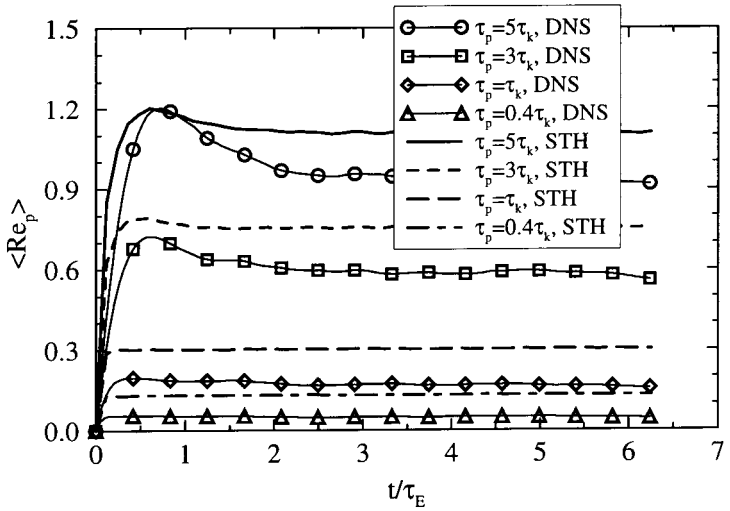

Fig. 4. Temporal variations of the mean particle Reynolds number for nonevaporating particles as calculated by stochastic and direct numerical simulations, in the absence of gravity.

stationary condition is much shorter in the stochastic simulations. (ii) For large particles, an overshoot is observed in the temporal variations of the particle Reynolds number, the extent of which is increased with the increase of the particle time constant. The stochastic model predicts a much smaller overshoot at the same particle time constant. (iii) The stationary values of the particle Reynolds number predicted by the stochastic model are larger than those via DNS. More importantly, the deviation observed between the stationary values depends on the particle time constant; the smaller the particle time constant the larger the deviation.

The influences of physics as itemized by (i)–(iii) are discussed by considering the temporal variations of the mean and higher order moments of $\tau_p^{1/2}$. This parameter is chosen since it is proportional to the particle diameter. First, we consider the temporal variations of the mean, the minimum, and the maximum values of $(\tau_p/\tau_{p0})^{1/2}$ for a case with $\tau_{p0} = 5\tau_k$, $\tau_{ec} = 5\tau_k$, and $Sc_p = 5$. The particles are initially injected into the flow with identical sizes and with the same velocity as that of their surrounding fluid elements. The particles are allowed to evaporate until the diameter of the smallest particle reaches 5% of its initial value at which time the simulation is terminated. Very small sizes are not considered to avoid the excessive computational requirements for particle tracking. Fig. 5 shows that the stochastic model predicts the mean diameter value very closely to DNS, especially during short and intermediate times. However, the minimum and maximum particle sizes predicted by the model deviate from those calculated by DNS. This can be explained by considering the variation of the particle Reynolds number with the particle time constant in Fig. 4. When the particle time constant varies from $0.4\tau_k$ to $5\tau_k$ the stationary values of the particle Reynolds number is increased by a factor of ~19 in DNS and ~8.3 in the stochastic simulations. Therefore, for the same size distribution, DNS predicts a much wider variation of the particle Reynolds number. Consequently, the variations of the evaporation rate is larger in DNS and a broader size distribution results. This also

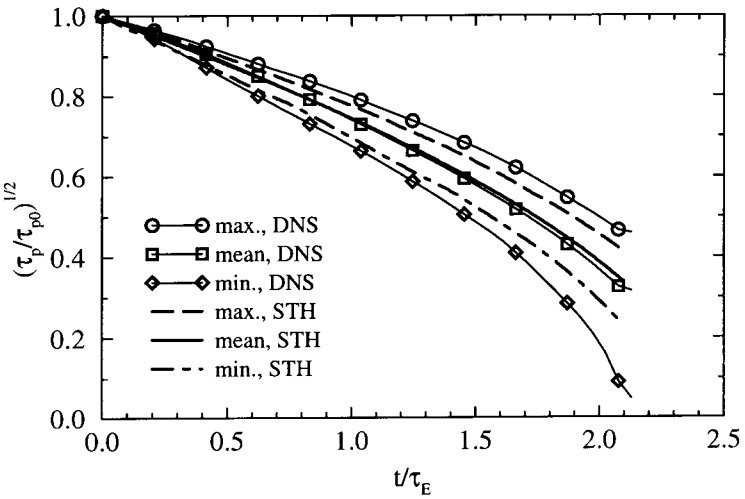

Fig. 5. Temporal variations of the minimum, the mean, and the maximum values of $(\tau_p/\tau_{p0})^{1/2}$ as calculated by stochastic and direct numerical simulations, $\tau_{p0} = 5\tau_k$, $\tau_{ec} = 5\tau_k$, and $Sc_p = 5$.

explains the sharper decrease of the minimum particle diameter at long times in DNS. It is noted that for a constant rate of change of τ_p (which is a reasonable assumption for the case considered here), $(d/dt)(\tau_p^{1/2}) \sim (\text{constant}/\tau_p^{1/2})$. Therefore, the rate of the diameter decrease becomes larger as the size of the particle is reduced.

Based on the discussion above, it is expected that the stochastic model predicts a narrower (thinner) size distribution than does DNS. This is evident in Fig. 6 which portrays the temporal variations of the standard deviation (σ) of $\tau_p^{1/2}$ for several Sc_p values. This figure shows that the stochastic model significantly underpredicts the standard deviation at intermediate and long times, although it is capable of predicting the right trend of variation with the particle Schmidt number. Three different regions are distinguished for each of the curves. The first region, for short times ($t/\tau_E < 0.2$), corresponds to the interval that the particle velocity is nonstationary. This period is characterized by small rates of growth of the standard deviations of $\tau_p^{1/2}$ as the particles are initially released with the same velocity as that of the surrounding fluid and the particle Reynolds number takes small values. Since the stochastic model predicts a larger variation of Re_p with the particle time constant in this nonstationary period (cf. Fig. 4), the standard deviations are higher in stochastic simulations during the initial short times—this is verified by considering the values near $t = 0$. In the second region ($0.2 < t/\tau_E < 2$), the particle Reynolds number adopts large values and the standard deviation increases more rapidly. In this region, the stochastic model underpredicts the DNS results as the model yields a smaller variation for the particle Reynolds number with the particle time constant. The third region ($t/\tau_E > 2$) is specified by the largest growth rates for the standard deviation. It is clearly seen in Fig. 6 that the model does not predict growth rates as large as those in DNS. This can be explained by the same argument provided earlier to explain the variations of the particle diameter at final times.

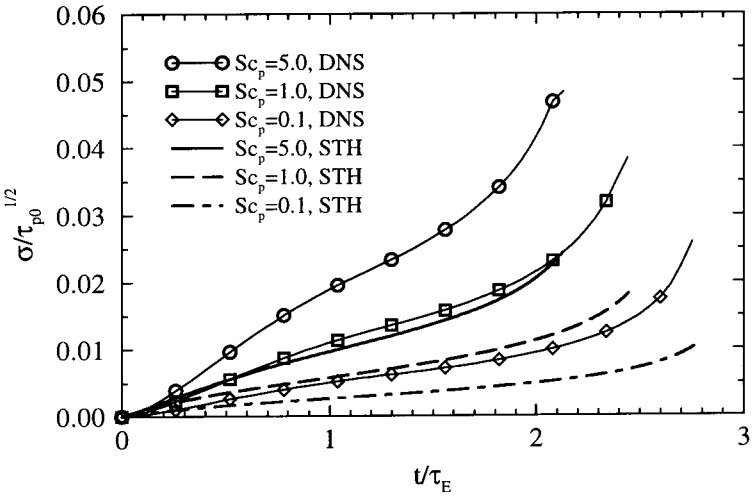

Fig. 6. Temporal variations of the standard deviation of $\tau_p^{1/2}$ as calculated by stochastic and direct numerical simulations at different particle Schmidt numbers. $\tau_{p0} = 5\tau_k$ and $\tau_{ec} = 5\tau_k$.

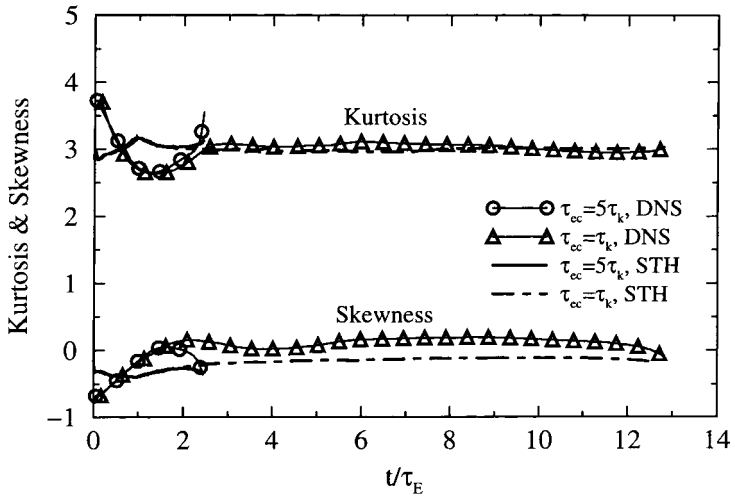

Fig. 7. Effects of the initial evaporation rate on the temporal variations of the skewness and kurtosis of $\tau_p^{1/2}$ as calculated by stochastic and direct numerical simulations, $\tau_{p0} = 5\tau_k$ and $Sc_p = 1$.

Fig. 7 shows the temporal variations of the skewness and kurtosis of $\tau_p^{1/2}$ for particles with $\tau_{p0} = 5\tau_k$ and $Sc_p = 1$ at two initial evaporation rates $\tau_{ec} = 5\tau_k$ and $\tau_{ec} = \tau_k$. The particles have initially zero velocity relative to the surrounding fluid; therefore, there is an initial time for the skewness and the kurtosis to reach stationary levels. In DNS, this time is about $2.5\tau_E$ which is about the same time required by nonevaporating particles to reach a stationary state (Fig. 4). The corresponding initial time in the stochastic simulations is about one eddy turnover time. As a result, the short time variations of both the skewness and the kurtosis are very different in DNS and stochastic simulations. At long times, for the case with smaller evaporation rate, the prediction of the stochastic model for the kurtosis is in good agreement with DNS results. However, the stochastic model underestimates the skewness values; it predicts a negative skewness throughout the duration of evaporation.

In general, the stochastic model predicts a narrower pdf of the droplet size than that obtained by DNS. This has a major impact on the evolution of the pdf when there is an initial size separation between the particles. In order to elaborate on this issue, we consider cases in which the initial particle size distribution consists of two distinct uniform-size groups of particles (i.e. the pdf of $\tau_p^{1/2}$ is double delta). In all of the cases, the particles are initially injected into the flow with a zero velocity relative to the local fluid, $\langle\tau_{p0}\rangle = 5\tau_k$, and $Sc_p = 1$. Fig. 8 shows the temporal evolution of the kurtosis of $\tau_p^{1/2}$ for cases with different initial standard deviations. After the onset of evaporation, there is a time delay before the two initially segregated branches of the pdf merge, resulting in the increase of the kurtosis. Fig. 8 indicates that this initial time delay depends on the initial separation between the two groups of particle sizes. As expected, the increase of this separation (the increase of σ_0) delays the merging. The stochastic model predicts a slower merging for all of the cases. This is due to the fact that the pdfs of each group of particles are predicted to be narrower (at any instant of time) in comparison to DNS.

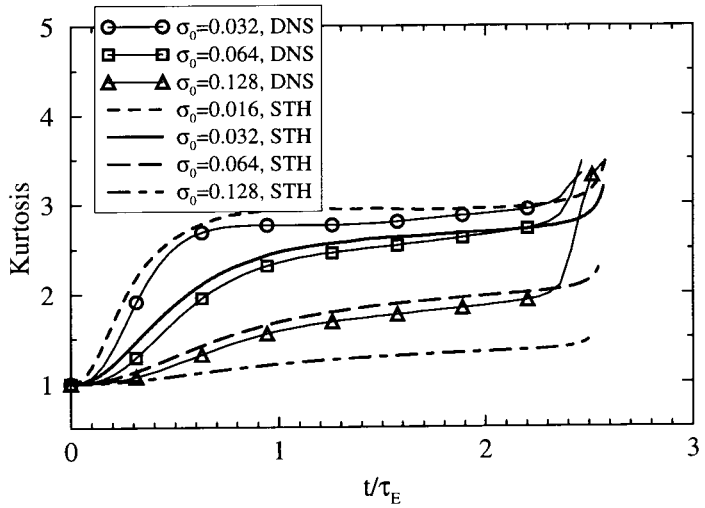

Fig. 8. Temporal variation of the kurtosis of $\tau_p^{1/2}$ for different initial standard deviations as calculated by stochastic and direct numerical simulations. $\langle\tau_{p0}\rangle = 5\tau_k$ and $\tau_{ec} = 5\tau_k$.

4. Comparison with theory

Mei et al. (1991) obtain a solution for the particle turbulence intensity and diffusion coefficient by assuming the form of the spectral density function as proposed by Kraichnan (1970). They consider contributions of all the forces acting on the particle but show that only the Stokes drag and the Basset forces need to be retained. In this section, their final results for cases in which the Basset force is neglected are compared with those predicted by the stochastic model.

The variations of the particle turbulence intensity with the particle time constant and the drift velocity are shown in Fig. 9. This figure indicates that the predictions via the stochastic model are in good agreement with those based on the theory for wide ranges of the particle time constant and the drift velocity. The stochastic model slightly underestimates the results via the theory in the absence of gravity while overpredicting these results at large drift velocity. The agreement between the two results diminishes with the decrease of the particle time constant. These trends are observed in both of the directions normal (Fig. 9a) and parallel (Fig. 9b) to the gravity direction. However, it must be emphasized that the predictions of the stochastic model is sensitive to the magnitude of C_2; values smaller than 0.73 were found to produce larger deviations from the theory.

In Fig. 10, comparisons are made between the predictions via the model and the theory for the asymptotic particle diffusivity coefficient at different drift velocities. The particle diffusivity coefficient is evaluated from (Hinze, 1975)

$$D^{p}_{\alpha\alpha}(t) = \frac{1}{2}\frac{d}{dt}\langle X^2_\alpha(t)\rangle \quad \alpha = 1, 2, 3 \tag{14}$$

The overall agreement is good. The stochastic model is capable of predicting the variations of the particle diffusivity coefficient with the drift velocity and with the particle time constant. In

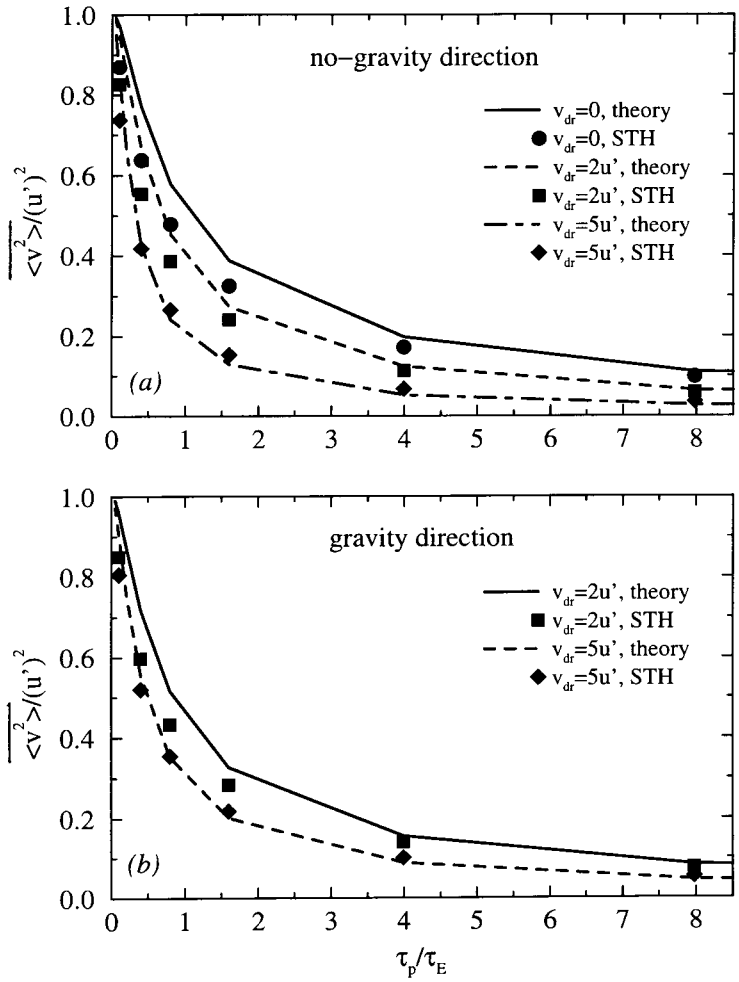

Fig. 9. Particle turbulence intensity from stochastic simulations and theory (Mei et al., 1991) in the direction (a) normal and (b) parallel to the gravity direction.

both the gravity and no-gravity directions, ε^p increases with the increase of the particle time constant when the drift velocity is small. The increase of the drift velocity tends to diminish the variations of ε^p with the particle time constant; an effect observed more strongly in the direction normal to the gravity direction.

As pointed out by Lu (1995), some of the earlier stochastic models do not correctly predict the increase of the long time particle diffusivity coefficient with the increase of the particle time constant. This is due mainly to the use of the "Lagrangian" autocorrelation. In order to show this, we also consider a Lagrangian stochastic model proposed by Lu et al. (1993). The results of the simulations are presented in Fig. 11 and indicate a decreasing trend for the long time particle diffusivity coefficient at zero gravity. The variations of ε^p at higher drift velocity values are, however, predicted correctly. In both the gravity and no-gravity directions the particle diffusivity coefficient becomes rather insensitive to the variations of the particle time constant.

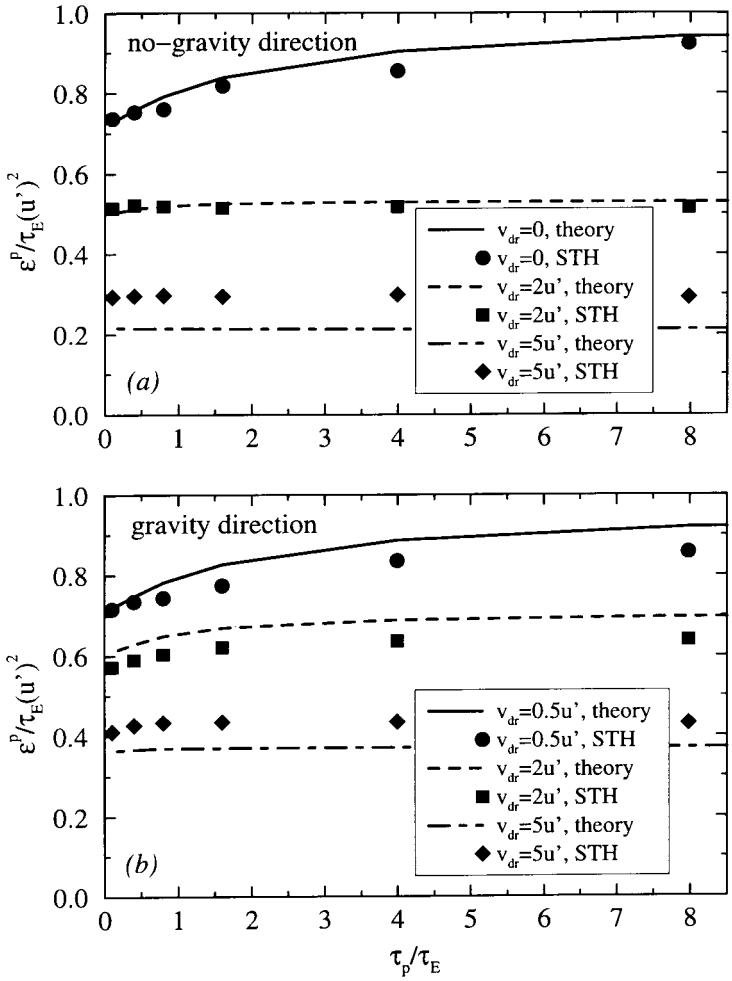

Fig. 10. Particle asymptotic diffusivity coefficient from stochastic simulations and theory (Mei et al., 1991) in the direction (a) normal and (b) parallel to the gravity direction.

It must be added here that the parameter C_2 does not appear in the Lagrangian model. However, the values of the particle diffusivity coefficient are indirectly dependent on C_2 as it relates τ_p to the "variable β" as used by Mei et al. (1991). Of course, C_2 only affects the magnitude of the particle diffusivity coefficient and does not change the decreasing trend observed at zero gravity.

The results presented in Figs. 9–11 are based on the assumption of Stokes drag with no modification for large particle Reynolds numbers. This assumption is necessary for comparison with the theoretical results of Mei et al. (1991) which are also based on the same assumption. However, in several of the cases the particle Reynolds number significantly exceeds unity. This will affect the particle intensity and diffusivity coefficient. In order to quantify these effects, in Table 1 the percentage relative differences between the results obtained with a modified drag relation (given in Eq. (8)) and those presented earlier based on the Stokes drag are provided.

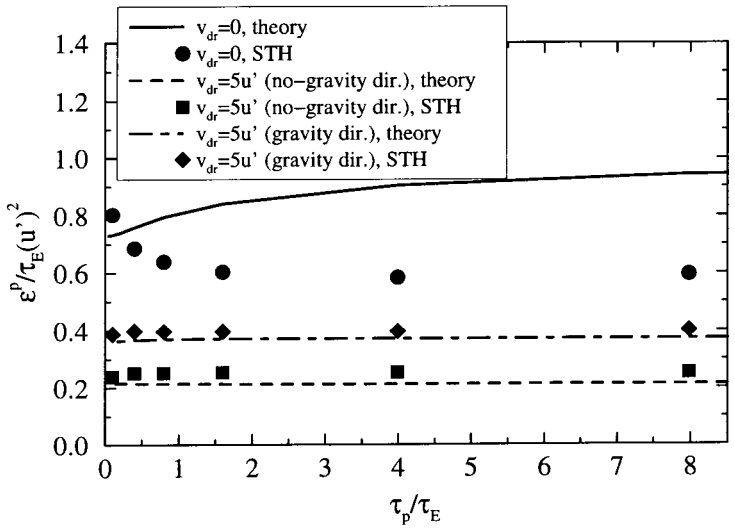

Fig. 11. Comparison of the results of the Lagrangian stochastic model and theory (Mei et al., 1991) for the particle asymptotic diffusivity coefficient.

As expected, the particle Reynolds number increases with the increase of the particle time constant and/or the drift velocity, resulting in larger deviations for the particle intensity and diffusivity coefficient at larger τ_p and v_{dr} values. It is noted that the particle diffusivity coefficient is predicted with a much smaller error than that associated with the particle intensity. This behavior is mostly due to the higher sensitivity of the particle intensity to the particle time constant. Regardless of the magnitude of the drift velocity, the particle intensity and diffusivity are predicted with comparable errors when the value of the particle time constant is small ($\tau_p = 0.1\tau_E$).

Table 1
Effects of the modified Stokes drag on the particle turbulence intensity and diffusivity. Subscripts "m" and "um" refer to the calculations based on the modified and unmodified (Stokes) drag, respectively. The particle intensity and diffusivity coefficient in cases with nonzero drift velocity belong to the gravity direction

$\frac{\tau_p}{\tau_E}$	$\frac{v_{dr}}{u'}$	$\langle \overline{Re_p} \rangle$	$\frac{\overline{\langle v_m^2 \rangle} - \overline{\langle v_{um}^2 \rangle}}{\overline{\langle v_{um}^2 \rangle}} \times 100$	$\frac{\overline{\langle \epsilon_m^p \rangle} - \overline{\langle \epsilon_{um}^p \rangle}}{\overline{\langle \epsilon_{um}^p \rangle}} \times 100$
0.1	0	0.22	0.8	0.0
0.4	0	0.69	4.4	0.7
1.6	0	1.86	16.0	1.4
8.0	0	4.83	42.0	2.0
0.1	2	0.72	2.6	2.3
0.4	2	1.40	10.4	4.9
1.6	2	2.83	30.7	6.0
8.0	2	6.21	76.5	13.5
0.1	5	1.62	6.3	7.8
0.4	5	2.90	24.0	11.0
1.6	5	5.24	67.7	19.4
8.0	5	10.19	153.2	32.8

5. Effects of gravity on evaporation

We now consider the effects of gravity on polydispersity of evaporating particles. In all the simulations considered in this section, the initial value of the particle time constant is fixed at $\tau_{p0} = 10\tau_k$, and a modified drag coefficient, Eq. (8), is used. The v_{dr} values given in this section refer to the magnitude of the drift velocity at the onset of evaporation. The temporal value of v_{dr} decreases proportional to the decrease of the droplet time constant such that the gravity constant, g, remains the same throughout each simulation.

Fig. 12 portrays the effects of gravity and evaporation on the velocity autocorrelation coefficient of both the heavy particle and its surrounding fluid particle (indicated by superscript

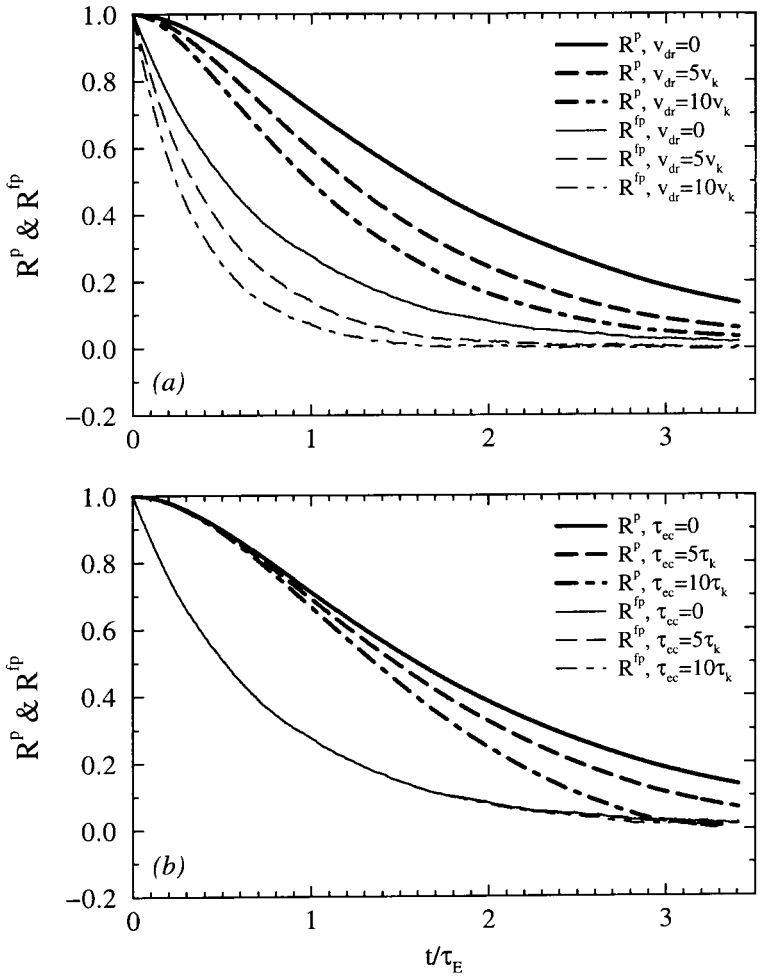

Fig. 12. Velocity autocorrelation coefficients of the heavy particle and its surrounding fluid particle. (a) Nonevaporating particles; effect of gravity. $\tau_p = 10\tau_k$. (b) Evaporating particles in zero gravity; effect of evaporation rate. $\tau_{p0} = 10\tau_k$ and $Sc_p = 0$.

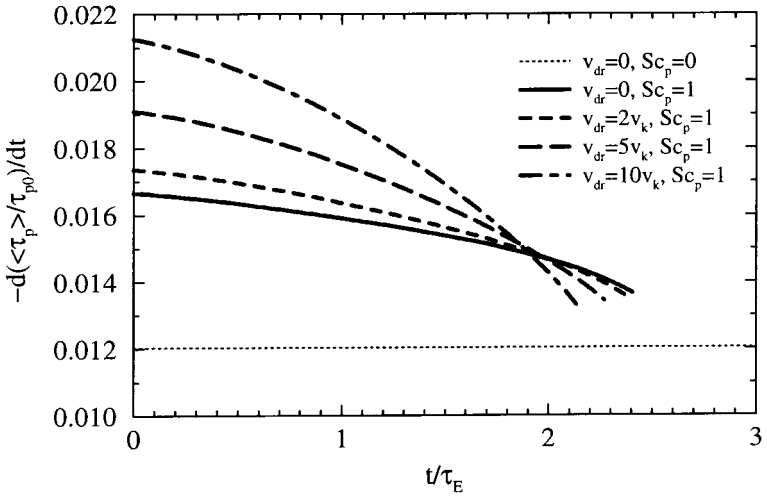

Fig. 13. Effects of the variations of the drift velocity on the depletion rate. $\tau_{p0} = 10\tau_k$ and $\tau_{ec} = 10\tau_k$.

"fp"). In Fig. 12a the velocity autocorrelations are given for nonevaporating particles at different drift velocities. As has been shown in previous studies (Wells and Stock, 1983; Mashayek et al. 1997) the increase of the drift velocity decreases the velocity autocorrelation of both the particle and its surrounding fluid due to the effect of crossing trajectories. Fig. 12b indicates that evaporation also results in a decrease of the particle velocity autocorrelation; the higher the evaporation rate, the smaller the particle velocity autocorrelation. This is due to the decrease of the particle size with evaporation. However, evaporation has virtually no effect on the velocity autocorrelation of the fluid. Therefore, the evaporating particle does not change its surrounding fluid as frequently as does the nonevaporating particle in a gravity environment.

The effects of gravity on the rate of evaporation are realized from Fig. 13 by considering the temporal variations of $-(\mathrm{d}(\langle\tau_p\rangle/\tau_{p0}))/\mathrm{d}t$ which is proportional to the depletion rate (k in Eq. (3)). When the nonlinear term in C_{Re} is zero (the case with $Sc_p = 0$ in Fig. 13), the evaporation rate is constant as expected. The inclusion of the nonlinear term increases the rate of evaporation. However, for all of the drift velocities, the rate of evaporation decreases nonlinearly in time due to the decrease of the particle size and, consequently, the particle Reynolds number. For short and intermediate times, the evaporation rate increases with the drift velocity as the particle Reynolds number is increased with the increase of the drift velocity. The larger evaporation rate at higher drift velocity results in a faster decrease of the particle size. As a result, a decreasing trend is observed for the variation of the evaporation rate with the drift velocity at long times.

An interesting behavior is observed in the variations of the standard deviation of $\tau_p^{1/2}$ with the increase of the drift velocity. Fig. 14a, for $\tau_{ec} = 10\tau_k$, shows that by increasing the drift velocity from zero to $2v_k$, the standard deviation increases at all times. However, further increase of the drift velocity results in an opposite trend. At large drift velocities the particle Reynolds number takes large values. This has the effect of diminishing the relative differences in the Reynolds number of different particles and results in a narrower $\tau_p^{1/2}$ pdf. A similar behavior is observed for the skewness of $\tau_p^{1/2}$ in Fig. 14b which shows that skewness is largest

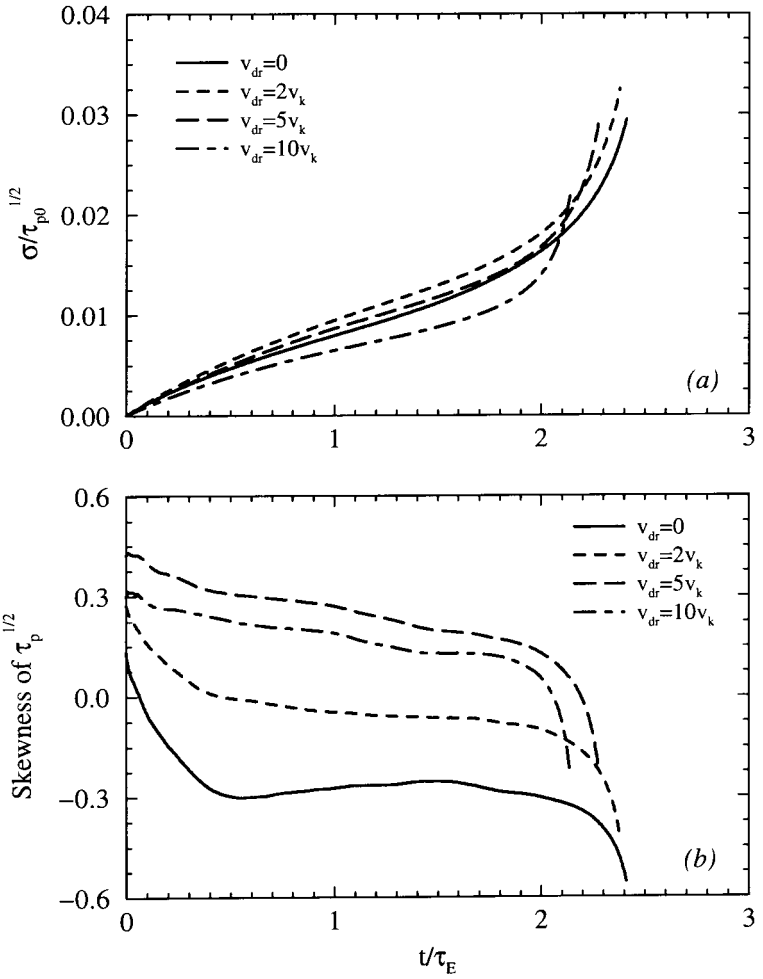

Fig. 14. Effects of the variations of the drift velocity on (a) the standard deviation and (b) the skewness of $\tau_p^{1/2}$. $\tau_{p0} = 10\tau_k$, $\tau_{ec} = 10\tau_k$, and $Sc_p = 1$.

at $v_{dr} = 5v_k$. Also, the increase of the drift velocity results in skewness of $\tau_p^{1/2}$ towards larger particles. Therefore, with the increase of the drift velocity, first the pdfs become wider and more skewed towards large particles. Further increase of the drift velocity results in an opposite trend.

When the rate of evaporation is decreased to $\tau_{ec} = 1$, Fig. 15 shows that the variations of the standard deviation and skewness of $\tau_p^{1/2}$ with the drift velocity change significantly. A monotonic decrease of the standard deviation with the increase of the drift velocity is observed at intermediate times. The skewness approaches near zero values for all drift velocities, before it sharply decreases (Fig. 15b). An examination of the standard deviation and skewness of $\tau_p^{1/2}$ for cases with $Sc_p = 5$ revealed no significant difference in their variations with the drift velocity when compared with those with $Sc_p = 1$.

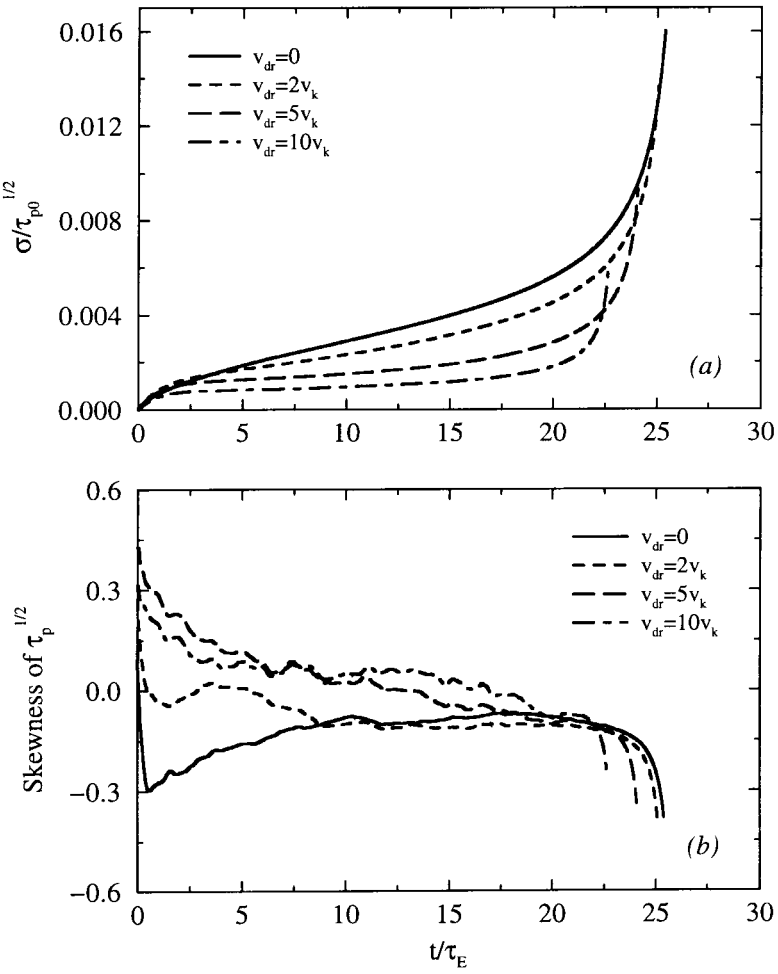

Fig. 15. Effects of the variations of the drift velocity on (a) the standard deviation and (b) the skewness of $\tau_p^{1/2}$. $\tau_{p0} = 10\tau_k$, $\tau_{ec} = \tau_k$, and $Sc_p = 1$.

Fig. 16 shows the temporal variation of the dispersion $\langle [X_\alpha(t) - X_\alpha(t=0)]^2 \rangle$. This figure indicates that dispersion decreases with the increase of the drift velocity in both of the directions parallel and normal to the gravity direction. Comparisons with the results of nonevaporating particles (thin lines) in Fig. 16 reveal that evaporation tends to decrease dispersion in low gravity environment and to increase it at higher drift velocities. This behavior is observed in both directions. It is also noted that the difference between the results under evaporating and nonevaporating conditions increases with time for all the drift velocities except $v_{dr} = 2v_k$ for which dispersion shows no apparent sensitivity to evaporation.

The temporal variations of dispersion for a case with $Sc_p = 5$ are shown in Fig. 17. Other parameters are the same as those considered for cases in Fig. 16. A comparison of these two figures reveals that the increase of the particle Schmidt number does not affect dispersion in the direction normal to the gravity direction. However, significant changes are

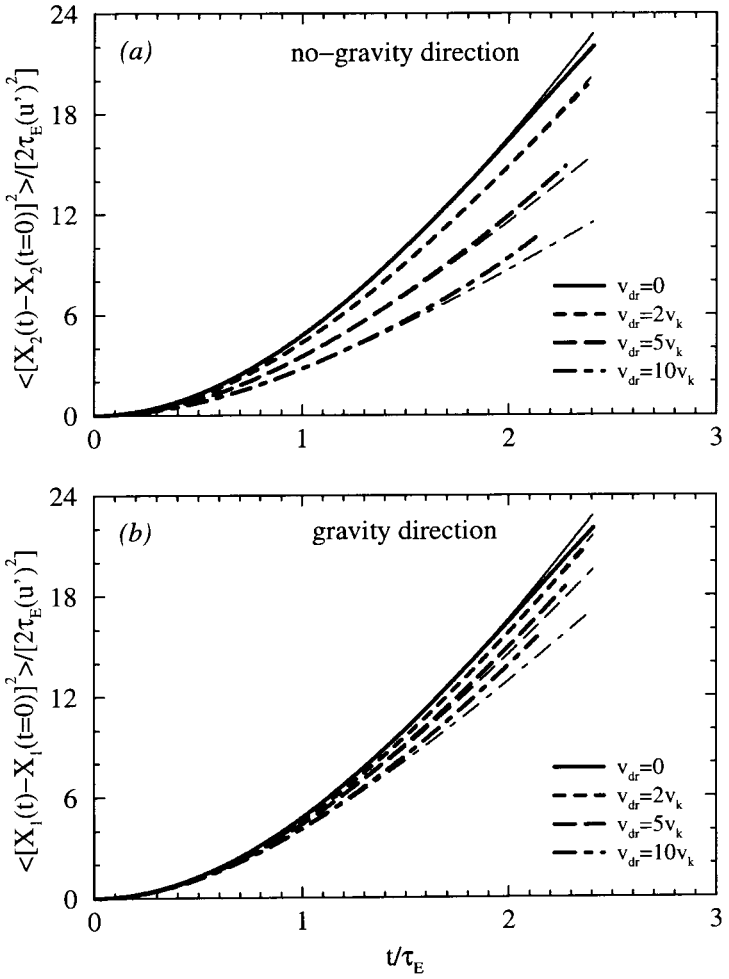

Fig. 16. Effects of the drift velocity on the dispersion of both nonevaporating (thin lines) and evaporating (thick lines) particles in the direction (a) normal and (b) parallel to the gravity direction. $\tau_{p0} = 10\tau_k$, $\tau_{ec} = 10\tau_k$, $Sc_p = 1$.

observed in the gravity direction. The effects of the particle Schmidt number on dispersion in the gravity direction is enhanced by increasing the drift velocity. It is also noted that similarly to the cases with $Sc_p = 1$, the case with $v_{dr} = 2v_k$ remains unaffected by evaporation.

6. Summary and concluding remarks

Results are presented of stochastic simulations of dispersion and polydispersity of particles in isotropic turbulent flows via the model proposed by Lu (1995). All of the empirical relations and the model's constant values are set the same as those suggested by Lu (1995). However, a

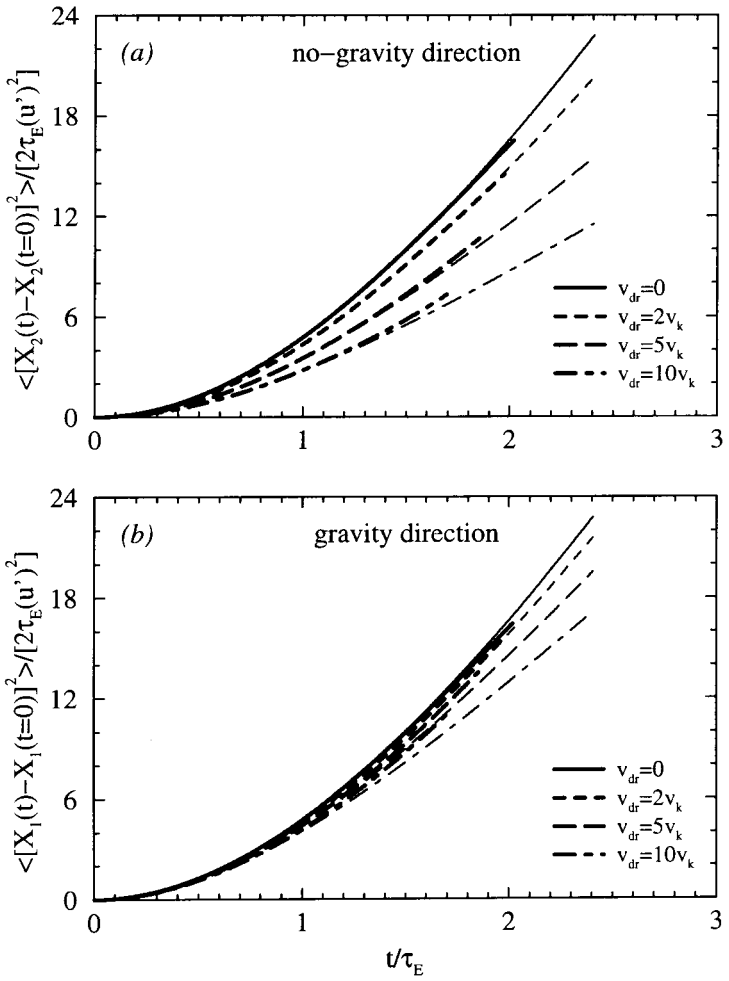

Fig. 17. Effects of the drift velocity on the dispersion of both nonevaporating (thin lines) and evaporating (thick lines) particles in the direction (a) normal and (b) parallel to the gravity direction. $\tau_{p0} = 10\tau_k$, $\tau_{ec} = 10\tau_k$, $Sc_p = 5$.

value larger than that suggested for the ratio of the Lagrangian and Eulerian integral time scales was necessary.

The predicted results via the model are compared with the results based on DNS (Mashayek et al., 1997) and theory (Mei et al., 1991). The stochastic model based on the Eulerian autocorrelation correctly predicts most of the trends observed by theory and DNS. When the model is constructed with a Lagrangian autocorrelation, the particle asymptotic diffusivity coefficient decreases with the increase of the particle time constant, in the absence of gravity. This trend is opposite of that predicted by the theory. A comparison of the particle velocity autocorrelation coefficients simulated by the Eulerian stochastic model with those by DNS indicates that the continuity effect (associated with the crossing trajectories effect) is not captured. Also, the peaking for the variation of the particle asymptotic diffusivity coefficient with the particle time constant as observed in DNS is not predicted. When compared with

DNS results, the model predictions exhibit better agreements for large particle time constants. The stochastic model is also used to quantify the effects of a modified drag relation on the particle turbulence intensity and the asymptotic diffusivity coefficient. The results suggest that the particle turbulence intensity is more sensitive to the drag calculations than is the particle diffusivity coefficient.

For evaporating particles, the stochastic model predicts thinner particle diameter pdfs than does DNS. This is mainly due to differences in the magnitudes of the particle Reynolds number in the two simulations. The higher order statistics of the particle size are calculated by the stochastic model and reasonable agreements are found with DNS. The model is also used to investigate the effects of gravity on evaporation. The depletion rate indicates an increasing trend with the increase of the drift velocity at small and intermediate evaporation times; an opposite trend is observed at long times. Furthermore, the variations of the standard deviation and the skewness of $\tau_p^{1/2}$ with the drift velocity is not monotonic. For small drift velocities, the standard deviation and the skewness increase with the increase of the drift velocity; an opposite trend is observed for large drift velocities.

It is important to note that the configuration of isotropic turbulence as considered here is much simpler than that in practical flow configurations. Therefore, weaker agreements between stochastic and DNS/experimental results may be expected when the model is implemented in inhomogeneous flows, especially those with large strain rates. Also, with extension and implementation of stochastic models to complex flows the problem associated with the (non)universality of the empirical constants must be resolved. Another important issue pertains to the number of particles for statistical sampling. Based on our experience, typically as many as 15,000 particles are necessary for reliable statistics. This could be a major restriction as in most of the reported applications of stochastic models to spatially inhomogeneous flows the total number of particles is significantly lower.

Acknowledgements

The author is grateful to Dr Q.Q. Lu for insightful discussions and to Professor R. Mei for providing the data used in Section 4. Part of this work was conducted when the author was at the State University of New York at Buffalo, working with Professor Peyman Givi and supported by the US Office of Naval Research under grant N00014-94-1-0667 with Dr Gabriel Roy as the Technical Monitor. Acknowledgement is made to the Donors of The Petroleum Research Fund, administered by the American Chemical Society, for partial support of this research. Computational resources were in part provided by the San Diego Supercomputing Center, the SEAS Computing Center at SUNY-Buffalo, and the College of Engineering Computer Facility at the University of Hawaii at Manoa.

References

Berlemont, A., Desjonqueres, P., Gouesbet, G., 1990. Particle Lagrangian simulation in turbulent flows. Int. J. Multiphase Flow 16, 19–34.

Berlemont, A., Grancher, M-S., Gouesbet, G., 1991. On the Lagrangian simulation of turbulence influence on droplet evaporation. Int. J. Heat Mass Transfer 34, 2805–2812.
Box, G.E.P., Jenkins, G.M., 1976. Time Series Analysis. Holden-Day, Oakland, CA.
Clift, R., Grace, J.R., Weber, M.E., 1978. Bubbles, drops, and Particles. Academic Press, New York.
Csanady, G.T., 1963. Turbulent diffusion of heavy particles in the atmosphere. J. Atmos. Sci. 20, 201–208.
Elghobashi, S., Truesdell, G.C., 1992. Direct simulation of particle dispersion in a decaying isotropic turbulence. J. Fluid Mech. 242, 655–700.
Gosman, A.D., Ioannides, E., 1981. Aspects of computer simulation of liquid-fuelled combustors, 81-0323. AIAA paper.
Graham, D.I., James, P.W., 1996. Turbulent dispersion of particles using eddy interaction models. Int. J. Multiphase Flow 22, 157–175.
Hinze, J.O., 1975. Turbulence. McGraw-Hill, New York.
Kraichnan, R.H., 1970. Diffusion by a random velocity field. Phys. Fluids 13, 22–31.
Lu, Q.Q., 1995. An approach to modeling particle motion in turbulent flows—I. Homogeneous, isotropic turbulence. Atmos. Environ. 29, 423–436.
Lu, Q.Q., Fontaine, J.R., Aubertin, G., 1993. A Lagrangian model for solid particles in turbulent flows. Int. J. Multiphase Flow 19, 347–367.
Mashayek, F., Jaberi, F.A., Miller, R.S., Givi, P., 1997. Dispersion and polydispersity of droplets in stationary isotropic turbulence. Int. J. Multiphase Flow 23, 337–355.
Maxey, M.R., Riley, J.J., 1983. Equation of motion for a small rigid sphere in a nonuniform flow. Phys. Fluids 26, 883–889.
Mei, R., Adrian, R.J., Hanratty, T.J., 1991. Particle dispersion in isotropic turbulence under Stokes drag and basset force with gravitational settling. J. Fluid Mech. 225, 481–495.
Ormancey, A., Martinon, J., 1984. Prediction of particle dispersion in turbulent flows. PhysicoChem. Hydrodyn. 5, 229–244.
Parthasarathy, R.N., Faeth, G.M., 1990. Turbulent dispersion of particles in self-generated homogeneous turbulence. J. Fluid Mech. 220, 515–537.
Pismen, L.M., Nir, A., 1978. On the motion of suspended particles in stationary homogeneous turbulence. J. Fluid Mech. 84, 193–206.
Ranz, W.E., Marshall, W.R., 1952. Evaporation from drops. Chem. Engng Prog. 48, 141–173.
Shearer, A.J., Tamura, H., Faeth, G.M., 1979. Evaluation of locally homogeneous flow model of spray evaporation. J. Energy 3, 271–278.
Shuen, J-S., Solomon, A.S.P., Zhang, Q-F., Faeth, G.M., 1983. A theoretical and experimental study of turbulent particle-laden jets, 168293. NASA CR.
Shuen, J-S., Solomon, A.S.P., Zhang, Q-F., Faeth, G.M., 1985. Structure of particle-laden jets: measurements and predictions. AIAA J. 23, 396–404.
Snyder, W.H., Lumley, J.L., 1971. Some measurements of particle velocity autocorrelation functions in a turbulent flow. J. Fluid Mech. 48, 41–47.
Solomon, A.S.P., Shuen, J-S., Zhang, Q-F., Faeth, G.M., 1984. A theoretical and experimental study of turbulent evaporating sprays, 174760. NASA CR.
Spalding, D.B. 1953. The combustion of liquid fuels. In: Proceedings of 4th Symposium (International) on Combustion. The Combustion Institute, Baltimore, MD. pp. 847–864.
Turns, S.R., 1996. An Introduction to Combustion: Concepts and Applications. McGraw-Hill, New York.
Wang, L-P., Maxey, M.R., 1993. Settling velocity and concentration distribution of heavy particles in isotropic turbulence. J. Fluid Mech. 256, 27–68.
Wells, M.R., Stock, D.E., 1983. The effects of crossing trajectories on the dispersion of particles in a turbulent flow. J. Fluid Mech. 136, 31–62.